



Reconstruction of Holocene and Last Interglacial vegetation dynamics and wildfire activity in southern Siberia

Jade Margerum¹, Julia Homann², Stuart Umbo¹, Gernot Nehrke³, Thorsten Hoffmann², Anton Vaks⁴, Aleksandr Kononov^{5,6}, Alexander Osintsev⁷, Alena Giesche⁸, Andrew Mason⁹, Franziska A. Lechleitner¹⁰, Gideon M. Henderson⁹, Ola Kwiecien¹, and Sebastian F. M. Breitenbach¹

¹Department of Earth and Environmental Sciences, Northumbria University, Newcastle-Upon-Tyne, NE1 8ST, UK

²Department Chemie, Johannes Gutenberg-Universität Mainz, Duesbergweg 10–14, 55128 Mainz, Germany

³Alfred Wegener Institut Helmholtz-Zentrum für Polar- und Meeresforschung, Section Marine BioGeoSciences, 27570 Bremerhaven, Germany

⁴Geochemistry and Environmental Geology Division, Geological Survey of Israel, 32 Yeshayahu Leibowitz Street, 9692100 Jerusalem, Israel

⁵Irkutsk National Research Technical University, Irkutsk, 664074, Russia

⁶Institute of the Earth's Crust, Russian Academy of Sciences, Siberian Branch, Irkutsk, 664033, Russia

⁷Speleoclub Arabika, St. Mamina-Sibiryaka 6a, 664058 Irkutsk, Russia

⁸U.S. Geological Survey, Alaska Science Center, Anchorage, Alaska 99508, USA

⁹Department of Earth Sciences, University of Oxford, South Parks Road, OX1 3AN Oxford, UK

¹⁰Department of Chemistry, Biochemistry and Pharmaceutical Sciences & Oeschger Centre for Climate Change Research, Universität Bern, Freiestrasse 3, 3012 Bern, Switzerland

Correspondence: Jade Margerum (jade.margerum@northumbria.ac.uk)

Received: 6 June 2024 – Discussion started: 12 June 2024

Revised: 25 September 2024 – Accepted: 16 December 2024 – Published: 20 March 2025

Abstract. Wildfires are a rapidly increasing threat to boreal forests. While our understanding of the drivers behind wildfires and their environmental impact is growing, it is mostly limited to the observational period. Here we focus on the boreal forests of southern Siberia and exploit a U–Th-dated stalagmite from Botovskaya Cave, located in the upper Lena region of southern Siberia, to document wildfire activity and vegetation dynamics during parts of two warm periods: the Last Interglacial (LIG; specifically part of the Last Interglacial maximum between 124.1 and 118.8 ka) and the Holocene (10–0 ka). Our record is based on levoglucosan (Lev), a biomarker sensitive to biomass burning, and on lignin oxidation products (LOPs) that discriminate between open and closed forest and hard- or softwood vegetation. In addition, we used carbonate carbon stable isotope ratios ($\delta^{13}\text{C}$), which reflect a dominant control of the host rock, to evaluate soil respiration and local infiltration changes. Our LOP data suggest that, during the Last Interglacial, the region around Botovskaya Cave was characterised by open for-

est, which by ca. 121.5 ka underwent a transition from fire-resistant hardwood to fire-prone softwood. The Lev record indicates that fire activity was high and increased towards the end of Last Interglacial just before 119 ka. In contrast, the Holocene was characterised by a closed-forest environment with mixed hard- and softwood vegetation. Holocene fire activity varied but at a much lower level than during the Last Interglacial. We attribute the changes in wildfire activity during the intervals of interest to the interplay between vegetation and climate. The open forests of the Last Interglacial were more likely to ignite than their closed Holocene equivalents, and their flammability was aided by warmer and drier summers and a stronger seasonal temperature contrast due to the increase in seasonal insolation difference compared to the Holocene. Our comparison of the last two interglacial intervals suggests that, with increasing global temperatures, the boreal forest of southern Siberia may become progressively more vulnerable to higher wildfire activity.

1 Introduction

Ongoing global warming results in (pan)regional changes in hydrological and temperature seasonality (Brunello et al., 2019; Swain, 2021), cryosphere extent (Kamp et al., 2022; Schuur et al., 2022), and the composition of the global biosphere (Steffen et al., 2018). These changes collectively affect the recurrence and intensity of droughts (Laaha et al., 2017) and wildfires (Schuur et al., 2022; Westerling et al., 2006). Global changes in vegetation and wildfire have far-reaching consequences, including further deterioration of biodiversity, and result in a positive feedback loop between fires, vegetation vulnerability, and climate change (Bowman et al., 2020; Cochrane and Bowman, 2021; Senande-Rivera et al., 2022). The combined effects of global warming and land-use change increase the flammability of many landscapes worldwide (Bowman et al., 2020), but the future magnitude and environmental consequences of wildfires at regional to local scales remain unclear.

According to global climate model projections, the fire-prone area of all boreal zones is likely to increase by the end of the 21st century (Senande-Rivera et al., 2022). Boreal forests of the Northern Hemisphere already show a trend to more frequent and intense wildfires (Kharuk et al., 2021, 2023; Walker et al., 2019). Siberia, hosting permafrost and boreal forest, two recently redefined climate tipping elements (Armstrong McKay et al., 2022), is a region that is highly vulnerable to rising temperature–wildfire positive feedback. Fire activity in Siberia is highest between April and September, and it is influenced by meteorological conditions such as temperature, precipitation, humidity, and wind speed, as well as land cover type, fuel availability (vegetation), and stand structure (tree species size and distribution) (Forkel et al., 2012; Tomshin and Solovyev, 2022). In the southern Siberian boreal forest belt, mean annual air temperatures have increased at twice the rate of the global terrestrial average and have accelerated since the early 1990s, driving the increase in forest fires (Balzter et al., 2007; Lugina et al., 2006; Talucci et al., 2022). The powerful Siberian heatwaves in 2010, 2020, and 2021, facilitated by elevated summer temperatures, led to aggravated wildfire activity that has been linked to anthropogenic climate change (Ciavarella et al., 2021; Hantemirov et al., 2022).

Increased wildfire activity has been identified as a potential driver of intensified permafrost thaw (Ciavarella et al., 2021; Talucci et al., 2022) and slowed forest recovery after burning (Ponomarev et al., 2016; Sun et al., 2021). A higher frequency of wildfires could transform boreal forests from carbon sinks to sources (Brazhnik et al., 2017; Dolman et al., 2012; Masyagina and Menyailo, 2020). Therefore, understanding the future of wildfires and their causes and effects demands an approach that integrates the monitoring of recent occurrences (collecting metrics data like fire seasonality, intensity, severity, and area) with insights from palaeo-fire research (particularly focused on past thermal maxima

with conditions similar to those expected over the coming decades). Currently, our knowledge of palaeo-wildfire behaviour in the Siberian boreal ecosystem is limited to northern regions based on reconstructions from ice cores (Eichler et al., 2011) and on charcoal, black carbon, and anhydrite records in lake sediments (Dietze et al., 2020; Glückler et al., 2021, 2022), which identify climate, wildfire activity, and vegetation type back to ca. 430 ka. In southern Siberia, observational data (e.g. remote-sensing data of burned area) are only available since the early 2000s (Bondur et al., 2023; García-Lázaro et al., 2018), and the sole study that explores regional wildfire and vegetation changes in the past is limited to the Holocene (Barhoumi et al., 2021).

Speleothems (i.e. secondary cave carbonate deposits, like stalagmites and flowstones) offer a large array of environmentally sensitive proxies (i.e. stable isotopes and trace elements) that inform on past hydrological, environmental, and climatic changes. Levoglucosan (Lev) is a monosaccharide biomarker that is solely produced through the combustion of cellulose at temperatures between 150 and 350 °C (Simoneit et al., 1999) and has been widely applied as a proxy for wildfire activity in various palaeoclimatic archives, like ice cores and lake sediments (Segato et al., 2021; Zennaro et al., 2014). Lev has recently been utilised in speleothems (Homann et al., 2022, 2023), where, as a compound embedded in secondary cave carbonates, it remains stable and protected from erosion or degradation over long time periods. Lev can represent both locally sourced, i.e. tens of kilometres, and/or efficiently transported Lev aerosols (Zennaro et al., 2014).

Lignins are naturally occurring biopolymers that are found in terrestrial vascular plants (Jex et al., 2014) and are well preserved during transport from soil to cave and within speleothem carbonate (Heidke et al., 2018). Lignin oxidation products (LOPs) are categorised as cinnamyl (C), syringyl (S), and vanillyl (V). The C / V and S / V ratios delineate different vegetation types, such as woody vs. non-woody and hardwoods vs. softwoods (Jex et al., 2014), respectively. Consequently, the combination of Lev and LOPs from the same archive can provide insights into the frequency of local wildfires and the type of vegetation (fuel) that was burning.

We present a wildfire and vegetation reconstruction for southern Siberia outside the Lake Baikal macroclimate zone for the Holocene and the second half of the Last Interglacial (LIG). Comparing our record with regional reconstructions places past fire activity in a wider environmental framework. Finally, we evaluate the relationship between wildfire activity and vegetation type during these two interglacial periods, comparing and contrasting Holocene and Last Interglacial conditions from a perspective of recent warming.

2 Material and methods

2.1 Study site

Botovskaya Cave (55.2994° N, 105.4445° E) is in southern Siberia, Russia, 250 km northwest of Lake Baikal (Fig. 1). The cave is on a south-facing slope at 750 m above sea level (a.s.l.) (for details, see supplemental data in Vaks et al., 2013, 2020), where valley and river elevations in this area are ca. 380 m a.s.l. The overlying bedrock geology comprises Ordovician (488.3–443.7 Ma) limestone and sandstone. The cave is 20–40 m below the surface and consists of a myriad of (sub)horizontal passages created by phreatic widening of tectonic faults and fractures, of which > 70 km has been mapped (Appendix A, Fig. A1). The mean cave air temperature was monitored between 2010 and 2018 and fluctuates between 1.6 and 1.9 °C in warmer areas (confined to cave passages within ca. 50 m from any entrance) and stays just above 0 °C in colder areas (poorly ventilated passages) of the cave (Appendix B, Fig. B1) (Vaks et al., 2013, 2020). Today, speleothems grow actively in only a few areas, and inactive speleothem formations are widespread and often broken through frost action. The cave is overlain by isolated patches of permafrost (Fig. 1) and soils showing strong similarities to burozems (Golubtsov et al., 2023) and umbric Albeluvisols/Podzoluvisols/Luvisols (Granina et al., 2019). The soils are between 15 and 45 cm deep and can be defined as grey-brown residual carbonate soils with added humus (Kozlova et al., 2021).

Our study region is characterised by a continental climate, with short, cool summers and severe, dry winters (Dwc climate in the Köppen-Geiger classification; Peel et al., 2007). Regional atmospheric circulation and climate in southern Siberia are influenced by the Atlantic westerlies that bring moisture eastwards and the Siberian High that dominates atmospheric circulation between autumn and spring and facilitates dry conditions by blocking moisture derived from the westerlies (Kostrova et al., 2020). During summer, the Siberian High weakens and is replaced by the Asiatic Low, and warm and unstable air masses cause heavy rainstorms between July and August. The mean annual precipitation is 345 mm in the nearby town of Zhigalovo (55 km south of Botovskaya Cave, ca. 420 m a.s.l.), of which 55 % falls between June and August. The cave site may be wetter because it is located a few hundred metres higher. Mean monthly summer and winter temperatures at the nearby Zhigalovo meteorological station, recorded between the late 1930s to 1990s, were 15.3 ± 1.2 and -26 ± 3.6 °C, respectively, but, in recent years (2000–2019), mean monthly summer temperatures have increased by > 1 to 16.7 ± 1.2 °C and winter temperatures by nearly 2 to -24.2 ± 3.9 °C. Local air temperatures (2010–2016) recorded just outside the entrance to Botovskaya Cave were higher compared to the Zhigalovo meteorological station, which is located in the Lena River valley, where frequent temperature inversions result in colder

mean air temperatures than at the higher-altitude Botovskaya Cave.

The plateau above the cave is characterised by a sub-boreal closed-canopy taiga forest, consisting of both gymnosperm (softwood) and angiosperm (hardwood) trees. Softwood species include larch (*Larix sibirica* Ledeb), fir (*Abies sibirica* Ledeb), Siberian cedar pine (*Pinus sibirica* Ledeb), and Scots pine (*Pinus sylvestris* L.), while hardwood species include birch (*Betula* spp. L.), aspen (*Populus tremula* L.), and cherry (*Prunus* spp. L.). The understorey is represented by shrub species such as redcurrant (*Ribes rubrum* L.) and blackcurrant (*Ribes nigrum* L.), as well as mosses, lichen, and liverwort (Ponomarev et al., 2016).

2.2 Sample description and mineralogy

Sample SB_pk7497-1, a 11 cm long stalagmite (Fig. 2), was found broken in a hydrologically active location ca. 1.1 km from the central entrance of Botovskaya Cave (see Appendix A, Fig. A1). The sample was sliced along the growth axis to provide two halves, one of which was used to perform all measurements required for this study. A macroscopically discernible detrital layer at 71.5 mm from the top of the sample marks a hiatus. It is possible that the SB_pk7497-1 record extended back further; however, the sample was found broken, and we were unable to locate any older segment in the cave. This specimen was utilised in previous studies to establish the history of permafrost and glacial–interglacial cyclicity of the past 500 000 years in Siberia (Vaks et al., 2013), using U-series-dated samples, and to investigate carbon cycle dynamics during permafrost thaw using carbon isotopes $\delta^{13}\text{C}$ and ^{14}C , trace element concentrations, and petrographic analyses (Lechleitner et al., 2020).

The mineral species calcite and aragonite were identified at the Alfred Wegener Institute Helmholtz Centre for Polar and Marine Research, Germany, using confocal Raman microspectrometry to map the growth axis. A total of 13 Raman spectra were measured using an excitation wavelength of ~ 480 nm, a spectrometer grating of 1800 g mm^{-1} , a 500 nm blaze, and an integration time of 0.05 s. The obtained maps each measured ca. 17.5 mm by 4 mm and were used for correction of stable isotope data (see Sect. 3.5).

2.3 Radiometric dating

Seven U–Th samples were milled with a 1 mm tungsten carbide drill bit and measured for dates at the University of Oxford, UK. The dates were previously published in Vaks et al. (2013, 2020). Contamination was minimised by milling and discarding the top ca. 50 μm of the sample surface before milling the powder for analysis. The U–Th dates and hiatus location and proxy data were input into the COPRA software routine (Breitenbach et al., 2012) to construct an age–depth model along the speleothem growth axis and extrapolate dates outside of the milled range.

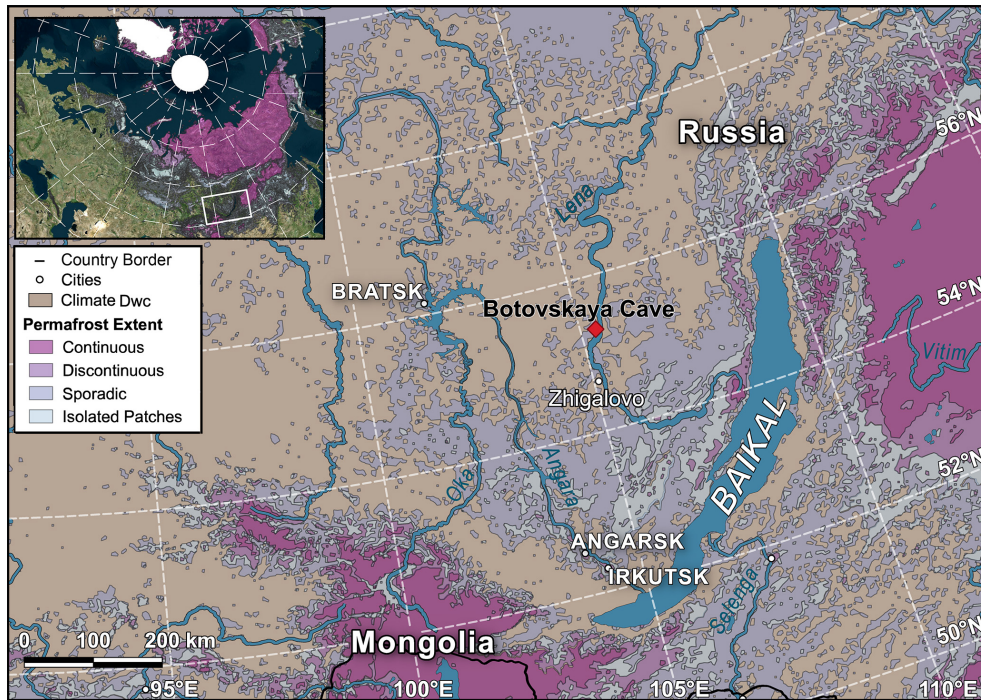


Figure 1. Location of Botovskaya Cave in southern Siberia, Russia. Permafrost zones within our study area are derived from modelled permafrost probabilities (Obu et al., 2019). Botovskaya Cave is within the zone of sporadic permafrost. Base aerial data: © Microsoft.

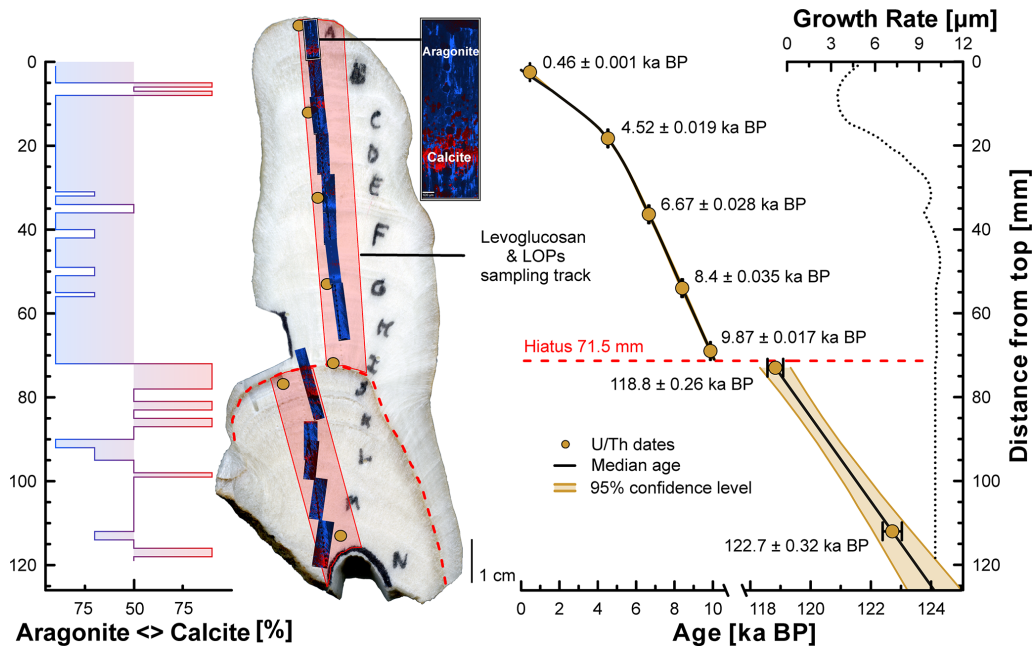


Figure 2. Distribution of U–Th dates and age uncertainties along stalagmite SB_pk7497-1. The COPRA median age model (black line) is constrained by seven U-series dates (gold circles with 2 s error bars). The hiatus is shown as a dashed red line. The golden lines and shading highlight the 95 % confidence bounds of the age–depth model. The growth rate varies from ca. $9.8 \mu\text{m a}^{-1}$ during the LIG and early Holocene to ca. $3.4 \mu\text{m a}^{-1}$ in the late Holocene (dotted black line). The red shaded area shows the sampling area for levoglucosan and lignin. Raman maps were taken along the growth axis and depict aragonite (blue) and calcite (red) sections (overlay on stalagmite scan). Enlarged images are shown in Appendix C (Fig. C1).

2.4 Levoglucosan and lignin sample preparation

A total of 40 subsamples weighing 500 ± 80 mg were milled at ca. 3 mm resolution from SB_pk7497-1 at Northumbria University, UK, for levoglucosan and lignin analyses. Of these, 20 subsamples originated from above the hiatus and 20 from below (Fig. 2). All subsequent sample preparation and analyses were completed at Johannes Gutenberg University Mainz, Germany.

Levoglucosan and LOP analyses were conducted following the methodology described by Homann et al. (2022). In short, the pulverised samples were spiked with $^{13}\text{C}_6$ levoglucosan, extracted with methanol, and evaporated in salinated vials. The evaporated residue was redissolved and filtered to $0.2 \mu\text{m}$, resulting in 40 samples prepared for measurement of levoglucosan concentrations. The remaining sample carbonate left over from the levoglucosan extraction was dried and dissolved in hydrochloric acid, and polymeric lignin was extracted using hydrophilic–lipophilic balance (HLB) solid-phase extraction (SPE), a technique which is used to separate and concentrate analytes. Because of the large samples required for lignin analysis, it was necessary to combine adjacent samples used in levoglucosan analysis (i.e. 1–2, 3–4, 5–6, etc.), resulting in only 20 samples prepared for lignin measurements. Lignin samples were eluted using methanol, which was evaporated, then the residue was subjected to an oxidative digestion to produce the phenolic compounds from the lignin (vanillyl, syringyl, and cinnamyl), and the resultant LOPs were extracted from solution with another SPE. Solutions were filtered to $0.2 \mu\text{m}$ prior to analysis. Levoglucosan and LOP analyses were conducted on a Dionex UltiMate 3000 ultrahigh-performance liquid chromatography system coupled to a heated electrospray ionisation source and a Q Exactive Orbitrap high-resolution mass spectrometer.

2.5 Stable carbon isotopes

Subsamples for stable carbon isotopes were taken at 1 mm resolution across the central growth axis of SB_pk7497-1 (oxygen isotopes were run concurrently but are not further presented here; see Sect. 3.5). Of a total of 116 samples taken, 73 were above and 43 were below the hiatus. Carbonate powders of $30\text{--}60 \mu\text{g}$ were measured with a Thermo Fisher Scientific Delta V Plus mass spectrometer, coupled to a ConFlo IV and a Thermo Finnigan Gasbench II at ETH Zurich, following the methodology of Breitenbach and Bernasconi (2011) and Spötl (2004). All isotope values were calibrated against Vienna Pee Dee Belemnite (VPDB) and reported in delta notation. Analytical uncertainties were $< 0.06\text{‰}$ (1σ) for $\delta^{13}\text{C}$. Because calcite and aragonite, or a mixture of both, are observed in the stalagmite, isotope results were corrected using the Raman maps. All results were corrected for their predominant mineralogy using the fractionation factors and methods proposed in Fohlmeister et al. (2018).

3 Results

3.1 Stalagmite fabric and mineralogy

Stalagmite mineralogy was identified by Raman mapping as predominantly aragonite, with frequent transitions between both calcite and aragonite especially in the lower half (Fig. 2). Occasionally, there are regions where mineral composition is uniformly distributed within the growth layer.

3.2 Radiometric dating and age–depth model

SB_pk7497-1 yielded five dates analogous with the Holocene and two Last Interglacial (LIG) dates (Fig. 2). These dates do not cover the entirety of the Holocene (0–11.7 ka) or LIG (115–130 ka) but rather intervals within these periods, specifically between 0 to 10 ka and 118.8 to 122.7 ka. From here, when referring to the Holocene and LIG (unless stated otherwise), these terms will refer to the intervals covered by our age-modelled dates as indicated below. The high U content (36–158 ppm) in this stalagmite yielded low age uncertainties of ≤ 50 years for the Holocene (younger than 9.87 ka) and < 320 years prior to 118.8 ka (Last Interglacial). Based on the COPRA model, the stalagmite was actively growing from the middle LIG (124.1 ka) through the late LIG (118.8 ka) and resumed growth in the early Holocene (9.9 ka) until almost the present day (0.3 ka). There was no evidence suggesting that the growth rate of SB_pk7497-1 changed from low and stable during the LIG, suggesting the extrapolation of ages outside the U-series dates is reliable. The mean Holocene growth rate was $8.4 \mu\text{m a}^{-1}$, whereas, during the LIG, it was higher at $\sim 10 \mu\text{m a}^{-1}$.

3.3 Levoglucosan

Levoglucosan (Lev) sampling resolution of ca. 90 years was achieved for the LIG, and a resolution of ca. 140 years was achieved for the Holocene. Lev concentrations range between 4.7 to 8.8 ng g^{-1} in the LIG, compared with 1.2 to 2 ng g^{-1} during the Holocene (Fig. 3a). LIG Lev concentrations remain relatively stable between 124 and 121 ka. The lowest LIG concentration (5.2 ng g^{-1}) was measured in the interval corresponding to 121–119.5 ka. The end of our LIG record at 118.8 ka is marked by a near doubling in Lev concentration to 8.8 ng g^{-1} . This marks the highest Lev concentration measured in our stalagmite.

Holocene Lev concentrations are relatively stable and have a lower average (1.7 ng g^{-1}) compared to the LIG (6 ng g^{-1}) (Fig. 3a). The highest values of 2 ng g^{-1} occur in the early Holocene between 10 and 9 ka, followed by low-amplitude changes around 1.5 ng g^{-1} . The lowest Lev values during the Holocene are observed at 5 and between 4 and 1.9 ka.

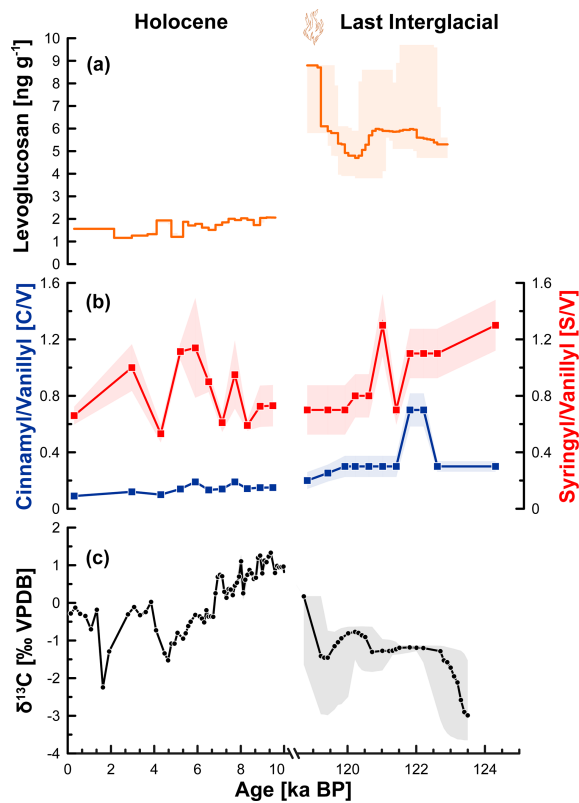


Figure 3. (a) Median levoglucosan concentration (orange line) with 95 % confidence intervals (shaded area). (b) Median C / V (blue) and S / V (red) ratios with 1σ error margins (shaded area). (c) Median $\delta^{13}\text{C}$ (black) with 95 % confidence intervals (shaded area). Confidence intervals were derived from 2000 Monte Carlo simulations in the COPRA age-modelling calculations and incorporate the interpolation and transfer of age uncertainty into the proxy domain. Error was negligible during the Holocene in panels (a), (b) (CV), and (c).

3.4 Lignin oxidation products (LOPs)

LOP sampling resolution was ca. 200 years for the LIG and 280 years for the Holocene. Concentration ratios are based on the phenolic structure of syringyl (S), cinnamyl (C), and vanillyl (V) (Fig. 3b). S / V ratios exhibit values constrained between 0.5 and 1.5 with variability in both the LIG and Holocene, in contrast to the C / V ratios, which are generally higher (0.2–1.2) during the LIG compared to the Holocene (< 0.2).

The LIG is characterised by a gradual decrease in the S / V ratio, while the C / V ratio remains relatively constant, aside from a positive excursion between 122.5 and 122 ka and a decline after 120 ka (Fig. 3b). We find the lowest C / V and S / V ratios of the LIG at 119 ka, before our record is interrupted by the onset of glacial conditions. The late LIG S / V and C / V ratios are similar to those found in the early Holocene. Holocene C / V ratios show low variability, whereas S / V ratios show high variability on millen-

nial timescales. The lowest C / V ratios are measured in the youngest section of the record.

3.5 Carbon stable isotopes

Across the LIG and the Holocene, $\delta^{13}\text{C}$ varies between -3‰ and 1‰ . The LIG carbon stable isotope record (Fig. 3c) broadly shows a 2‰ – 3‰ shift towards less negative values between 124 to 118.8 ka. During the early Holocene (until 4.6 ka), the $\delta^{13}\text{C}$ values show a long-term decrease between 1.3‰ to -1.5‰ overlaid by short-term variability. The late Holocene (after 5 ka) shows a shift to less negative values (ca. -0.6‰), punctuated by one excursion between 1.9 and 1.6 ka to lower values between -1.3‰ to -2.2‰ . Presently, the robust interpretation of $\delta^{18}\text{O}$ data is hindered by insufficient information from other moisture- and temperature-related proxies, and here we discuss only vegetation-related $\delta^{13}\text{C}$ data.

4 Discussion

Lev and lignin proxy records from Siberian stalagmites offer new insights into interglacial vegetation composition and wildfire recurrence in understudied southern Siberia. The dominant vegetation type in the region surrounding a cave can be identified using the ratios of LOPs extracted from speleothems (Homann et al., 2022). In determining the vegetation type (softwood vs. hardwood, woody vs. non-woody), we follow the classification by Hedges and Mann (1979). Hardwood and softwood vegetation can be distinguished by elevated and reduced S / V ratios, respectively (Fig. 4). Low C / V ratios indicate woody plants, while high C / V ratios reflect non-woody open vegetation. Hardwood vs. softwood and woody vs. non-woody plants differ in flammability and in recovery time after burning (Tepley et al., 2018); hence knowing the vegetation composition (fuel) is an important factor in understanding past wildfire dynamics. Furthermore, wildfire activity (i.e. temporal dynamics) can be revealed by levoglucosan (Lev) concentration in palaeoenvironmental time series.

Lev has been explored as a wildfire proxy in various environmental archives (i.e. ice cores and lake sediments), but its use in speleothems is still novel, and aspects like transport and preservation are currently being investigated. As Lev is unstable at higher temperatures, it is an indicator of smouldering fires (as opposed to flaming combustion), which involve lower temperatures and slower, flameless fires (Simoneit et al., 1999). These types of smouldering fires are more common in and characteristic of boreal ecosystems, leading to an underrepresentation of high-intensity flaming fires (Zennaro et al., 2014). However, any underrepresentation of high-intensity wildfires emphasises the need for complementary proxies, such as charcoal particles or polycyclic aromatic hydrocarbons (PAHs), which can provide a fuller picture of the fire regime for both low- and high-temperature

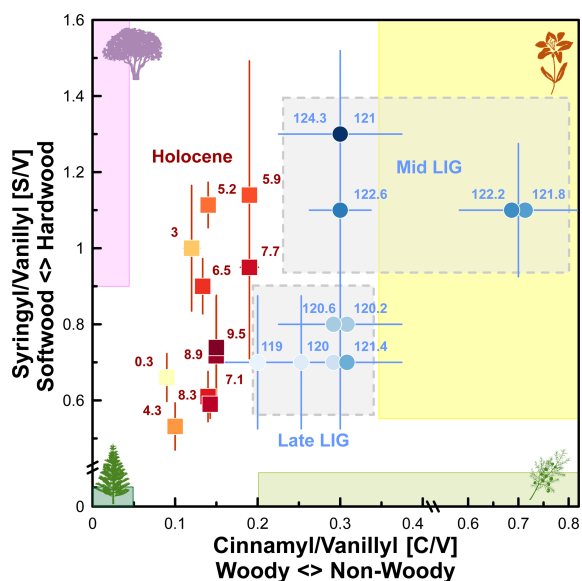


Figure 4. Stalagmite-based S / V vs. C / V ratios reflect changes in vegetation composition during the Last Interglacial (LIG) and the Holocene. Samples are colour-coded by age, with darker colours indicative of older samples. The red points are Holocene samples, and the blue points are LIG samples. Overlapping samples were adjusted left/right for clarity (e.g. 122.2–121.8 ka). The shaded boxes denote experimentally determined LOP ratios of predominant species (Hedges and Mann, 1979): dark green is dominated by softwood woody plants, light green is dominated by softwood non-woody plants, pink denotes hardwood woody plants, and yellow indicates hardwood non-woody plants. Regions generally characterised by the mid-LIG and late LIG are highlighted by shaded grey boxes. The Holocene is characterised by more woody vegetation compared to the LIG. Icons (pine tree, juniper bush, flower, and deciduous tree) are all sourced from <https://www.freepik.com> (last access: 19 May 2023).

fires (Argiriadis et al., 2024). Another concern regarding Lev is how the transport mechanisms (i.e. water routing) between surface location(s) to speleothem might change over time, along with post-depositional alteration and degradation of the archived signal. The large difference of 2.5 ng g^{-1} between the LIG and Holocene cautions that Lev may reflect a varying growth rate and/or changes in water flow path (e.g. caused by permafrost during the growth hiatus) between ca. 115 and 11.7 ka. These concerns can be addressed if trends are verified by replication of the wildfire reconstruction from other stalagmites from the same cave, which is currently unfeasible, or comparison of trends in our other proxies that we would expect to act similarly, thus showing similar differences between the Holocene and LIG. We find that our $\delta^{13}\text{C}$ record retains similar values in both periods, suggesting transport pathways did not change and that Lev can be interpreted as a real fire signal. We also found no relation between Lev and mineralogical variations between aragonite and calcite.

Both vegetation composition and wildfire activity differ between the LIG and the Holocene, painting a picture of a sparsely forested and fire-prone environment during the LIG and a forested and fire-resilient environment during the Holocene. Our interpretation of the LOP, levoglucosan, and $\delta^{13}\text{C}$ records is supported by independent reconstructions of seasonal insolation (Laskar et al., 2004); Greenland air temperature (Andersen et al., 2004); and precipitation, temperature, and moisture estimates derived from Lake Baikal pollen profiles (Tarasov et al., 2005, 2007).

4.1 Last Interglacial vegetation composition and wildfire activity

Relatively high C / V values point to the dominance of non-woody taxa (steppe-like vegetation) during the mid LIG. High S / V values suggest that sparse woody taxa present were composed of hardwood species (e.g. birch and aspen) above Botovskaya Cave – species which are normally restricted by the presence of permafrost (Kharuk et al., 2023). Lev concentrations are also high at that time and signify high wildfire activity (Fig. 5b and c). According to a pollen-based quantitative reconstruction of LIG climate from Lake Baikal (Tarasov et al., 2007; Fig. 5e–g), southern Siberian mean temperatures of the warmest and coldest months during the LIG were ca. 17 and -22°C , respectively (vs. 15.3 and -26°C today), whereas global maximum annual temperatures were ca. 2°C warmer than the pre-industrial (Capron et al., 2014; Turney and Jones, 2010). The pollen data also indicate higher-than-present annual precipitation and moisture. We suggest that a warmer growth season in spring and summer (Fig. 5e), high summer insolation (Fig. 5h), and higher precipitation (Fig. 5f) allowed hardwood species to advance northward and begin occupying larger areas previously dominated by softwood. Hardwood species are less flammable in low-intensity fires (Bryukhanov et al., 2018) and reproduce and mature faster than their softwood counterparts following burning (Shvetsov et al., 2019). These adaptations facilitate rapid post-fire recolonisation and regrowth and constitute a competitive advantage over softwood species after burning (Belcher et al., 2021). Hardwood species like birch quickly replace softwood species such as larch after wildfires, while coniferous trees may take 80–120 years to return (Shvetsov et al., 2019). The high S / V values ca. 124 ka (Fig. 5b) likely reflect similar replacement dynamics. A modern analogue for this scenario can be found in today's steppe and forest steppe zones of southern Siberia, where high wildfire activity leads to expansion and succession of hardwood-dominated vegetation, with grasses, shrubs, and hardwood species quickly repopulating areas affected by wildfire and higher mortality of conifer seedlings (Kharuk et al., 2021; Tchebakova et al., 2009).

Declining C / V values and lower S / V values over the course of the later LIG (Fig. 5a and b) document a transition from steppe-like vegetation towards more closed-canopy

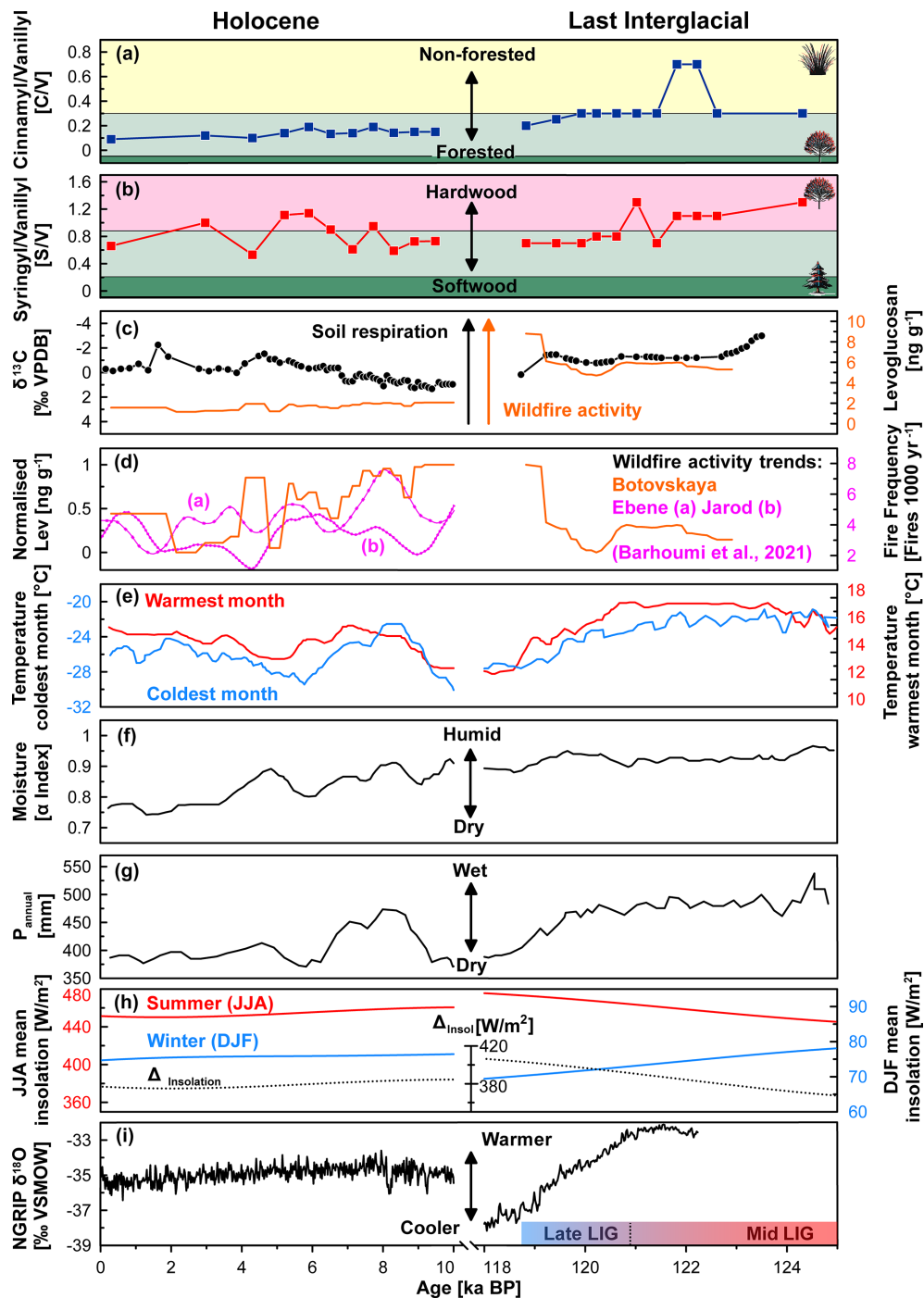


Figure 5. Vegetation (a, b), wildfire, and climate (c, d) signals derived from Botovskaya Cave shown with published regional and hemispheric records of vegetation and climate (d–i). (a) Dark-green shading indicates predominantly forested vegetation, yellow shading indicates open vegetation, and yellow/green shading indicates mixed vegetation. (b) Pink shading indicates hardwood, dark-green shading indicates softwood, and pink/green shading indicates mixed vegetation. (c) The $\delta^{13}\text{C}$ record reflects local hydrological conditions and soil respiration, with lower values indicating wetter conditions and increased soil respiration. (d) Normalised levoglucosan levels highlight multi-centennial trends during the LIG and the Holocene, and local wildfire records (Barhouri et al., 2021) from lakes Ebene (a) and Jarod (b) present fire frequency trends for the Holocene. Lake Baikal pollen records (Tarasov et al., 2007) include temperatures of the warmest and coldest months (e), moisture (f), and annual precipitation (g). (h) Hemispheric mean insolation at 55.3°N in June–August (JJA) on the left and December–February (DJF) on the right and Δ insolation (summer–winter) (Laskar et al., 2004) indicate changes in thermal seasonality. (i) The $\delta^{18}\text{O}$ ice core values from the North Greenland Ice Core Project (NGRIP) showing changes in Northern Hemisphere air temperature (Andersen et al., 2004).

forests and from hardwood to softwood. This type of vegetation is more susceptible to wildfire (Mensah et al., 2023), and the transition reflected in the LOP record is concomitant to an abrupt increase in Lev concentration that reflects increased wildfire activity ca. 119.2 ka. Regional climate records indicate that the late LIG became cooler and drier, with lower annual precipitation and available moisture and reduced surface temperatures (Tarasov et al., 2007; Fig. 5e–g). The insolation curve points to increasing temperature seasonality with colder winters and warmer summers, while the Greenland ice core record suggests hemispheric cooling (Andersen et al., 2004; Fig. 5h and i). The cooling triggered a vegetation transition to more softwood-dominated forests that were better adapted to drier summers and harsh winters. Because this vegetation type is more vulnerable to wildfires, these conditions likely supported more frequent and intense wildfires. The decrease in regional surface temperatures (Fig. 5e) ushered in the onset of the Last Glacial and eventually led to the return of continuous permafrost (which is supported by the cessation of speleothem growth after ca. 118.8 ka).

During a short period between 122.2 and 121.8 ka within the LIG, higher C / V values suggest a transition from woody to non-woody vegetation (e.g. grasslands) (Fig. 5a). This relatively short transition was likely a symptom of continuously high wildfire activity, as evidenced by increasing Lev concentrations. When forests burn frequently, higher fire-induced vegetation mortality can create patchy habitats, leading to the succession of pioneering non-woody vegetation and creating open spaces for grassland and meadows where forests usually stand (Kharuk et al., 2021). We suggest that this relatively short (ca. 400-year) period was a temporary transition when forests could not recover due to continuously high wildfire activity (in this case, likely higher frequency, as less woody vegetation burns more readily under drier conditions). The return to pre-excursion C / V values by ca. 121.5 ka suggests that wildfires were not frequent enough to induce a permanent transition to a non-forested, open landscape.

An abrupt increase in Lev concentrations after 119 ka indicates significantly increased wildfire activity (Fig. 5c). This could have been induced by drier and still warm summers in the late LIG that would have promoted dry lightning (the most common natural ignition source for wildfires in Siberia), which considerably increases the probability of wildfires (Hessilt et al., 2022). Alongside softwood prevalence, this would have supported the expansion of fire into wider areas. The observed increase in wildfire activity in the late LIG was facilitated by natural processes and not by humans, who likely arrived in the Lena River valley only during the Last Glacial (Shichi et al., 2023; Weber et al., 2011).

The outlined vegetation and wildfire dynamics are supported by our stalagmite $\delta^{13}\text{C}$ record that reflects the interplay between open vs. forested vegetation (as indicated by the C / V values), temperature (Fig. 5a–e), and soil respiration. A greater contribution of open vegetation (e.g. grass-

lands) during the LIG (Fig. 5a) would result in less negative $\delta^{13}\text{C}$ values (Fig. 5c). High summer temperatures dry out the topsoil and reduce soil respiration despite high precipitation events (thunderstorms), resulting in increasing $\delta^{13}\text{C}$ values (Fohlmeister et al., 2020). Increased drought stress in vegetation, as a result of higher temperatures, may add to the observed $\delta^{13}\text{C}$ trend (Fohlmeister et al., 2020). This is especially notable near the end of the LIG (118.8 ka), when, despite the prevalence of a more forested landscape (lower C / V ratios), high $\delta^{13}\text{C}$ values suggest that vegetation may have suffered from growth season drought and reduced productivity.

The LOP-based vegetation reconstruction for the LIG suggests an earlier transition from hardwood species to softwood species than regional reconstructions based on pollen data from Lake Baikal (e.g. Granoszewski et al., 2005; Tarasov et al., 2005, 2007). We observe a higher concentration of hardwood species during the mid-LIG (from 124 to 121 ka), whereas pollen records (Granoszewski et al., 2005) indicate less hardwood developed in the Baikal region between 123.8 and 118.8 ka. We argue that our reconstruction from Botovskaya Cave reflects relatively local vegetation dynamics that are separated from the Baikal Lake records by distance (250 km) and relatively high mountain ridges, while the lake record integrates a much larger catchment area that is more representative of general trends in southern Siberia.

4.2 Vegetation composition and wildfire activity during the Holocene

Reconstructed Holocene vegetation composition appears to resemble modern assemblage of trees and shrubs with mixed hard- and softwood taxa. Generally declining C / V values in the second half of the Holocene (Fig. 5a) suggest, independently of hard- and softwood vegetation types, that the forests of the later Holocene became better established and denser. Fluctuating S / V ratios indicate a changing prevalence of hardwood and softwood species over much of the Holocene (Figs. 4 and 5b).

Despite lower temperatures compared to the middle LIG (Fig. 5e and i), hardwood species found some foothold, likely due to a longer growth season facilitated by higher insolation in both summer and winter (Fig. 5h). Significantly lower Lev concentrations, compared to the LIG (Fig. 5c), indicate reduced fire prevalence, with a general decrease over the Holocene. Reduced moisture availability during the Holocene (Fig. 5f and g) relative to the LIG suggests a drier summer season with fewer thunderstorms (the main source of warm-season rainfall) and, consequently, a reduced chance of dry lightning (Hessilt et al., 2022).

While the Holocene fire activity appears subdued compared to the LIG, the normalised Lev record reveals pronounced multi-centennial-scale variability, superimposed on the long-term trend (Fig. 5d). Higher temperatures, moisture availability, and growth season precipitation (Fig. 5e–g and i)

during the Northern Hemisphere Holocene thermal maximum (Baker et al., 2017) likely facilitated more wildfires than during other portions of the Holocene. While higher moisture availability and increased wildfire activity seem, at first glance, counter-intuitive, increased temperatures and moisture can increase biomass (fuel) availability that can increase vulnerability to wildfire activity (Marlon, 2020). The seasonal temperature contrast remained relatively stable over the course of the Holocene, compared to the late LIG (Fig. 5h and i), which might have helped the establishment of denser forest cover. Our $\delta^{13}\text{C}$ record supports this interpretation, as the transition from high $\delta^{13}\text{C}$ values in the early Holocene to more negative $\delta^{13}\text{C}$ values in the middle Holocene can be interpreted as improved soil development and higher respiration under forest cover.

To date, only one Holocene wildfire record is available from southern Siberia (Barhoumi et al., 2021). The reconstruction is based on charcoal occurrence in two lakes located to the immediate southeast of Lake Baikal and suggests higher wildfire activity in the early Holocene, followed by an abrupt decline after 6.5 ka (Fig. 5d). Comparison with pollen records from the Lake Baikal region (Bezrukova et al., 2013; Demske et al., 2005; Shichi et al., 2009) indicates that this wildfire trend was likely related to a shift from predominantly Siberian spruce (*Picea obovata*) to pine trees (e.g. *Pinus sylvestris*), which drove a transition from mostly crown fires (entire trees) to more surface fires (surface litter and decaying understorey) by the middle Holocene. Our record presents an increased S/V value after 6.5 ka, which indicates mixed softwood and hardwood forest and agrees with vegetation shift to more pine trees as these species correspond to more open forests that eventually facilitate a higher hardwood abundance (Anyomi et al., 2022). While our record cannot identify wildfire intensity or estimate its vertical distribution (e.g. differentiating between crown and surface fires), their reconstruction confirms a generally decreasing fire activity trend over the Holocene in the wider Baikal region (Fig. 5c and d).

A slight increase in our Lev concentration record in the late Holocene (Fig. 5d) may reflect either increasing natural wildfire prevalence or, possibly, an increasing anthropogenic component. Human populations have been well established in the Baikal region since the Last Glacial (Weber et al., 2011; Shichi et al., 2023), with archaeological evidence (e.g. petroglyphs at Shishkino in the Lena valley) pointing to large river valleys, like those of the Angara and Lena, as main migration routes (Kılınç et al., 2021; Tolstoy, 1958; White et al., 2008). Palaeolithic humans likely had an impact on the environment from activities such as hunting, foraging, and use of fire (Barhoumi et al., 2021). Increasingly consequential activities (i.e. pastoralism and land clearing) were not evident until the mid-late Holocene, with no evidence of forest management during any period (Weber et al., 2011). Although our Holocene record might be influenced by human activity, we caution that our dataset lacks the temporal

resolution to identify anthropogenic impacts on fire occurrence. Increasing population density deep within Eurasia has been linked with elevated wildfire occurrence, and similar links might be found with early human settlements (White et al., 2008). However, the significantly higher wildfire activity in the late LIG period, with vegetation similar to the late Holocene, suggests that other factors, like warmer-than-modern surface temperatures and enhanced seasonal temperature contrasts, play a more important role.

The reconstructed Holocene vegetation shows trends similar to previously published pollen-derived datasets from the Lake Baikal region. We find a dominance of mixed softwood and hardwood in the early Holocene (ca. 10–8 ka), which aligns with records of established boreal forests with mixed species, including both softwood and hardwood species, in the Baikal region (Tarasov et al., 2007, 2009; Kobe et al., 2020, 2022; Demske et al., 2005). Distinct transitions to denser, hardwood-dominant forests at 7.8, 6.6–5.2, and 3 ka align loosely to cooling episodes (Demske et al., 2005) and a decline in softwood species more representative of open forests, such as larch (Kobe et al., 2022). Over the late Holocene (after ca. 4 ka) the reconstructed forest composed of a mix of hardwood and softwood remained similar to that in the early Holocene, although forests became denser, likely indicating a greater admixture of closed forest species, like spruce, fir, and Siberian pine (Kharuk et al., 2021). Pollen data from Lake Ochaul (Kobe et al., 2020), located ca. 100 km southeast of Botovskaya Cave, agree with our reconstruction and suggest an increasingly denser forested landscape and a high contribution of hardwood species (specifically birch), which is likely reflected in our dataset at hardwood-dominated intervals.

4.3 Comparison of wildfires and vegetation during the LIG and Holocene

Our data indicate that the LIG and Holocene differed in terms of fire pattern. Fire pattern and fire regime are often used interchangeably, and here we follow Bowman et al. (2020) and refer to fire pattern as the interplay between climate, vegetation type (fuel), and ignition (natural or related to human activity). Fire regime is defined as a typical range of fire frequency, type, intensity, severity, seasonality, and spatial scale (Cochrane and Bowman, 2021). Given the challenges in extracting these properties from speleothem archives, we have chosen to limit our reconstruction to fire pattern.

Contrasting vegetation types (i.e. wildfire fuel) during the LIG and Holocene seem to play a crucial role in wildfire activity in southern Siberia. Open steppe vegetation is more flammable than closed forest, and hardwoods are generally more resistant to wildfire than softwoods. As vegetation type is inherently related to regional climate, disentangling the primary driver for changes in wildfire pattern is complex.

Our data suggest that, during the LIG, fire activity increased with increasing seasonal temperature gradient

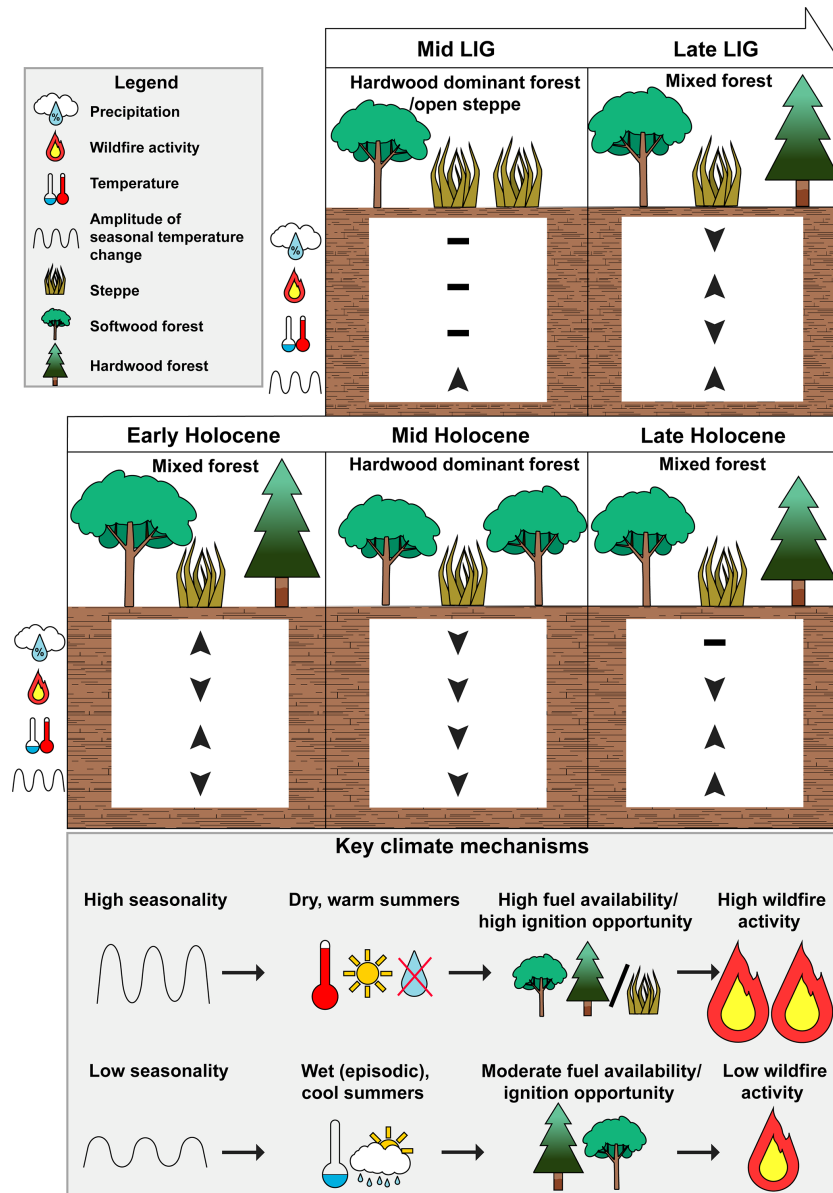


Figure 6. Schematic detailing the general trends summarised in Fig. 5. The arrows and horizontal lines in the upper (LIG) and middle (Holocene) panels summarise the overall trend in each parameter (precipitation, wildfire activity, temperature, and seasonal temperature change), with up, down, and horizontal lines denoting increasing, decreasing, and stable trends, respectively. The lower panel summarises the general mechanisms we identified that support wildfire activity and specify the hydrological and environmental parameters leading to both low and high wildfire activity in southern Siberia.

(Fig. 6). Fire ignition is more probable during warmer, drier summers in a steppe-like environment than in a forested landscape (Kharuk et al., 2021). High temperature and fuel availability are conducive to more frequent and severe wildfires. Seasonal hydrological dynamics are another important factor for wildfire activity, as the availability and temporal distribution of moisture during the growth season determine not only vegetation composition but also wildfire hazard (i.e. the likelihood of fire ignition by lightning) (Tchebakova et al., 2009).

Moisture supply to continental Eurasia via the westerlies depends on Atlantic Sea ice extent and atmospheric circulation patterns (Smith et al., 2016), which varied between the LIG and the Holocene due to differences in meridional temperature gradients (Baker et al., 2017). The Atlantic Multidecadal Oscillation has recently been found to influence wildfire regimes in northeastern China via the modulation of moisture supply and regional warming (Gao et al., 2021).

The relatively high $\delta^{13}\text{C}$ values (-2‰ to $+1\text{‰}$) during both the Holocene and the LIG indicate a significant con-

tribution from the host rock, rather than soil and vegetation overlying the cave. The very stable and lower (compared to Holocene) $\delta^{13}\text{C}$ values in the middle to late LIG likely reflect higher regional temperatures, as suggested by Fohlmeister et al. (2020), for environments with low (< 800 mm) annual precipitation. High wildfire activity and non-woody taxa during the LIG (Fig. 5a–c) align well with these dry and warm conditions. Soil respiration diminished further in the late LIG when sea ice (and eventually Scandinavian ice) build-up limited eastward moisture transport (Svendsen et al., 2004), as evidenced by the high $\delta^{13}\text{C}$ value at the end of our LIG record (ca. 119 ka).

Higher stalagmite $\delta^{13}\text{C}$ values during the early Holocene might result from more episodic summer rainfall and generally drier warm-season conditions with reduced soil respiration. These drier episodes induced a vegetation shift to more softwood, mostly mixed woody and non-woody vegetation, and higher wildfire activity as a consequence of increased fuel availability that promoted dry-lightning efficiency.

Considering the differences in vegetation dynamics, insolation, and moisture availability, the LIG is not an adequate analogue for the Holocene. However, with increasingly drier and warmer continental summers as a result of global warming (Zhang et al., 2020), and independent of orbital parameters, the boreal forest zone is likely to be more frequently exposed to summer heat waves that promote fire weather (Hessilt et al., 2022). Such conditions, enhanced by ongoing forest loss and vegetation shifts linked to wildfires, will likely fuel a positive feedback loop and further increase fire activity in the Eurasian boreal forest.

5 Conclusions

Stalagmite-derived levoglucosan (Lev) concentrations and lignin oxidation products (S / V and C / V ratios) allowed reconstruction of Last Interglacial (LIG) and Holocene wildfire and vegetation dynamics in southern Siberia. In the region, dry lightning is the most probable natural ignition mechanism of wildfires. Consequently, we have focused on two other elements of the fire triangle: vegetation (fuel) and climate. Our results document diverse landscapes surrounding Botovskaya Cave in the LIG and Holocene. The LIG was characterised by a mix of steppe and forest vegetation fuelling frequent and sustained wildfires. A gradual increase in seasonal temperature gradient and regional drying accompanied by transition from fire-resilient hardwood to fire-vulnerable softwood taxa were likely reasons for increased fire activity towards the end of the LIG. In contrast to the LIG, forest vegetation established during the Holocene demonstrates ongoing competition between hard- and softwood taxa. The mixed nature of Holocene forests, likely related to generally cooler Holocene temperatures and subdued seasonal temperature contrast, appears to have reduced wildfire activity compared to in the LIG. While the wildfire ac-

tivity varied over the course of the Holocene, the amplitude and absolute values were much lower compared to the LIG. We propose that the composition of the vegetation and the thermal contrast between the seasons are the most important natural drivers of southern Siberian wildfires. Under continued global warming, increasing summer temperatures and dryness are likely to promote more frequent wildfires, with escalating societal and ecological repercussions.

Appendix A

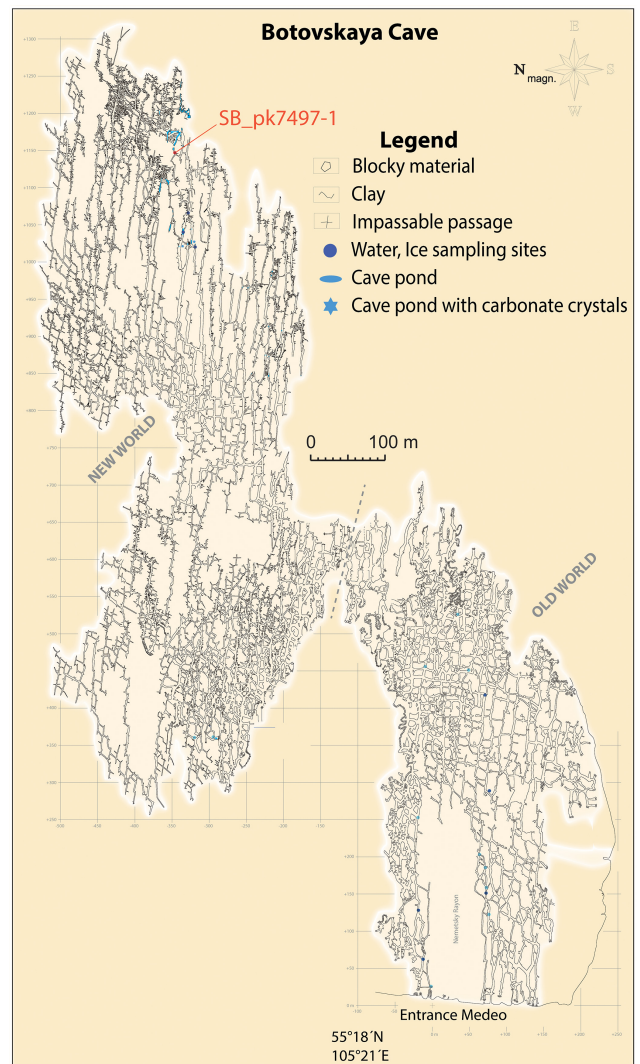


Figure A1. Mapped areas of Botovskaya Cave with locations of specimen. Old and New World regions are joined in the area crossed with a dashed grey line. The location of sample SB_pk7497-1 is highlighted in the northeastern part of the New World. Key features are listed within the figure.

Appendix B

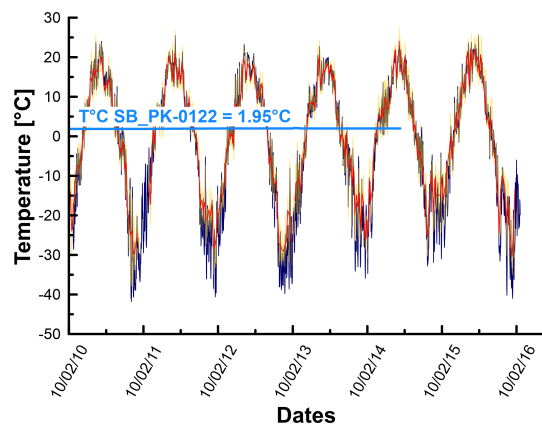


Figure B1. Temperatures recorded inside (light-blue line) and outside (yellow and red lines) Botovskaya Cave over a period of 6 years. Trends in both daily (yellow line) and weekly (red line) average temperatures outside the cave have increased since 2013, whereas inside mean cave temperatures remain stable. Average daily temperatures for Zhigalovo meteorology station (55 km south of Botovskaya; see Fig. 1) are recorded by the navy-blue line (Klein Tank et al., 2002).

Appendix C



Figure C1. All Raman maps and corresponding locations presenting aragonite (blue shades) and calcite (red shades) mineralogy along the growth axis of sample SB_pk7497-1.

Data availability. All results from this study are available in the Supplement to this publication.

Supplement. The supplement related to this article is available online at <https://doi.org/10.5194/cp-21-661-2025-supplement>.

Author contributions. Study design: JM, SFMB, and JH. Methodology and data acquisition: JM, SFMB, JH, GN, FAL, and AV. Original draft preparation: JM. Writing and editing: JM, SFMB, OK, AG, SU, FAL, GN, TH, AV, AK, AO, AM, and GMH.

Competing interests. The contact author has declared that none of the authors has any competing interests.

Disclaimer. Publisher's note: Copernicus Publications remains neutral with regard to jurisdictional claims made in the text, published maps, institutional affiliations, or any other geographical representation in this paper. While Copernicus Publications makes every effort to include appropriate place names, the final responsibility lies with the authors.

Acknowledgements. We thank members of Speleoclub Arabika and Tobias Braun for their help during fieldwork in Siberia and Hamish Couper for help with laboratory work for U/Th dating. We also thank Pavel Tarasov, Sina Longman, Frederic Wilson, and Natalie Latysh for providing helpful comments on the article. Any use of trade, firm, or product names is for descriptive purposes only and does not imply endorsement by the US Government.

Financial support. This research has been supported by the Leverhulme Trust (grant no. RPG-2020-334), the Deutsche Forschungsgemeinschaft (grant no. HO 1748/20-1), and the Natural Environment Research Council (grant nos. NE/G013829/1 and NE/S007512/1).

Review statement. This paper was edited by Mary Gagen and reviewed by Ramesh Glückler and two anonymous referees.

References

- Andersen, K. K., Azuma, N., Barnola, J.-M., Bigler, M., Biscaye, P., Caillon, N., Chappellaz, J., Clausen, H. B., Dahl-Jensen, D., Fischer, H., Flückiger, J., Fritzsche, D., Fujii, Y., Goto-Azuma, K., Grønbold, K., Gundestrup, N. S., Hansson, M., Huber, C., Hvidberg, C. S., Johnsen, S. J., Jonsell, U., Jouzel, J., Kipfstuhl, S., Landais, A., Leuenberger, M., Lorrain, R., Masson-Delmotte, V., Miller, H., Motoyama, H., Narita, H., Popp, T., Rasmussen, S. O., Raynaud, D., Rothlisberger, R., Ruth, U., Samyn, D., Schwander, J., Shoji, H., Siggard-Andersen, M.-L., Steffensen, J. P., Stocker, T., Sveinbjörnsdóttir, A. E., Svensson, A., Takata,

- M., Tison, J.-L., Thorsteinsson, Th., Watanabe, O., Wilhelms, F., White, J. W. C., and North Greenland Ice Core Project members: High-resolution record of Northern Hemisphere climate extending into the last interglacial period, *Nature*, 431, 147–151, <https://doi.org/10.1038/nature02805>, 2004.
- Anyomi, K. A., Neary, B., Chen, J., and Mayor, S. J.: A critical review of successional dynamics in boreal forests of North America, *Environ. Rev.*, 30, 563–594, <https://doi.org/10.1139/er-2021-0106>, 2022.
- Argiriadis, E., Denniston, R. F., Ondei, S., Bowman, D. M. J. S., Genuzio, G., Nguyen, H. Q. A., Thompson, J., Baltieri, M., Azenon, J., Cugley, J., Woods, D., Humphreys, W. F., and Barbante, C.: Polycyclic aromatic hydrocarbons in tropical Australian stalagmites: a framework for reconstructing paleofire activity, *Geochim. Cosmochim. Ac.*, 366, 250–266, <https://doi.org/10.1016/j.gca.2023.11.033>, 2024.
- Armstrong McKay, D. I., Staal, A., Abrams, J. F., Winkelmann, R., Sakschewski, B., Loriani, S., Fetzer, I., Cornell, S. E., Rockström, J., and Lenton, T. M.: Exceeding 1.5 °C global warming could trigger multiple climate tipping points, *Science*, 377, eabn7950, <https://doi.org/10.1126/science.abn7950>, 2022.
- Baker, J. L., Lachniet, M. S., Chervyatsova, O., Asmerom, Y., and Polyak, V. J.: Holocene warming in western continental Eurasia driven by glacial retreat and greenhouse forcing, *Nat. Geosci.*, 10, 430–435, <https://doi.org/10.1038/ngeo2953>, 2017.
- Balzter, H., Gerard, F., George, C., Weedon, G., Grey, W., Combal, B., Bartholomé, E., Bartalev, S., and Los, S.: Coupling of vegetation growing season anomalies and fire activity with hemispheric and regional-scale climate patterns in central and east Siberia, *J. Climate*, 20, 3713–3729, <https://doi.org/10.1175/JCLI4226>, 2007.
- Barhoumi, C., Vogel, M., Dugerdil, L., Limani, H., Joannin, S., Peyron, O., and Ali, A. A.: Holocene fire regime changes in the southern Lake Baikal region influenced by climate-vegetation-anthropogenic activity interactions, *Forests*, 12, 978, <https://doi.org/10.3390/f12080978>, 2021.
- Belcher, C. M., Mills, B. J. W., Vitali, R., Baker, S. J., Lenton, T. M., and Watson, A. J.: The rise of angiosperms strengthened fire feedbacks and improved the regulation of atmospheric oxygen, *Nat. Commun.*, 12, 503, <https://doi.org/10.1038/s41467-020-20772-2>, 2021.
- Bezrukova, E. V., Hildebrandt, S., Letunova, P. P., Ivanov, E. V., Orlova, L. A., Müller, S., and Tarasov, P. E.: Vegetation dynamics around Lake Baikal since the middle Holocene reconstructed from the pollen and botanical composition analyses of peat sediments: Implications for palaeoclimatic and archeological research, *Quatern. Int.*, 290–291, 35–45, <https://doi.org/10.1016/j.quaint.2012.10.043>, 2013.
- Bondur, V. G., Gordo, K. A., Voronova, O. S., Zima, A. L., and Feoktistova, N. V.: Intense wildfires in Russia over a 22 year period according to satellite data, *Fire*, 6, 99, <https://doi.org/10.3390/fire6030099>, 2023.
- Bowman, D. M. J. S., Kolden, C. A., Abatzoglou, J. T., Johnston, F. H., van der Werf, G. R., and Flannigan, M.: Vegetation fires in the Anthropocene, *Nat. Rev. Earth Environ.*, 1, 500–515, <https://doi.org/10.1038/s43017-020-0085-3>, 2020.
- Brazhnik, K., Hanley, C., and Shugart, H. H.: Simulating changes in fires and ecology of the 21st century Eurasian boreal forests of Siberia, *Forests*, 8, 49, <https://doi.org/10.3390/f8020049>, 2017.
- Breitenbach, S. F. M. and Bernasconi, S. M.: Carbon and oxygen isotope analysis of small carbonate samples (20 to 100 µg) with a GasBench II preparation device, *Rapid Commun. Mass Sp.*, 25, 1910–1914, <https://doi.org/10.1002/rcm.5052>, 2011.
- Breitenbach, S. F. M., Rehfeld, K., Goswami, B., Baldini, J. U. L., Ridley, H. E., Kennett, D. J., Prufer, K. M., Aquino, V. V., Asmerom, Y., Polyak, V. J., Cheng, H., Kurths, J., and Marwan, N.: COConstructing Proxy Records from Age models (CO-PRA), *Clim. Past*, 8, 1765–1779, <https://doi.org/10.5194/cp-8-1765-2012>, 2012.
- Brunello, C. F., Andermann, C., Helle, G., Comiti, F., Tonon, G., Tiwari, A., and Hovius, N.: Hydroclimatic seasonality recorded by tree ring $\delta^{18}\text{O}$ signature across a Himalayan altitudinal transect, *Earth Planet. Sc. Lett.*, 518, 148–159, <https://doi.org/10.1016/j.epsl.2019.04.030>, 2019.
- Bryukhanov, A. V., Panov, A. V., Ponomarev, E. I., and Sidenko, N. V.: Wildfire Impact on the Main Tree Species of the Near-Yenisei Siberia, *Izv. Atmos. Ocean. Phy.*, 54, 1525–1533, <https://doi.org/10.1134/S0001433818110026>, 2018.
- Capron, E., Govin, A., Stone, E. J., Masson-Delmotte, V., Mulitza, S., Otto-Bliesner, B., Rasmussen, T. L., Sime, L. C., Waelbroeck, C., and Wolff, E. W.: Temporal and spatial structure of multi-millennial temperature changes at high latitudes during the Last Interglacial, *Quaternary Sci. Rev.*, 103, 116–133, <https://doi.org/10.1016/j.quascirev.2014.08.018>, 2014.
- Ciavarella, A., Cotterill, D., Stott, P., Kew, S., Philip, S., van Oldenborgh, G. J., Skålevåg, A., Lorenz, P., Robin, Y., Otto, F., Hauser, M., Seneviratne, S. I., Lehner, F., and Zolina, O.: Prolonged Siberian heat of 2020 almost impossible without human influence, *Climatic Change*, 166, 9, <https://doi.org/10.1007/s10584-021-03052-w>, 2021.
- Cochrane, M. A. and Bowman, D. M. J. S.: Manage fire regimes, not fires, *Nat. Geosci.*, 14, 455–457, <https://doi.org/10.1038/s41561-021-00791-4>, 2021.
- Demske, D., Heumann, G., Granoszewski, W., Nita, M., Makakowa, K., Tarasov, P. E., and Oberhänsli, H.: Late glacial and Holocene vegetation and regional climate variability evidenced in high-resolution pollen records from Lake Baikal, *Global Planet. Change*, 46, 255–279, <https://doi.org/10.1016/j.gloplacha.2004.09.020>, 2005.
- Dietze, E., Mangelsdorf, K., Andreev, A., Karger, C., Schreuder, L. T., Hopmans, E. C., Rach, O., Sachse, D., Wennrich, V., and Herzsuh, U.: Relationships between low-temperature fires, climate and vegetation during three late glacials and interglacials of the last 430 kyr in northeastern Siberia reconstructed from monosaccharide anhydrides in Lake El'gygytgyn sediments, *Clim. Past*, 16, 799–818, <https://doi.org/10.5194/cp-16-799-2020>, 2020.
- Dolman, A. J., Shvidenko, A., Schepaschenko, D., Ciais, P., Tchepakova, N., Chen, T., van der Molen, M. K., Belelli Marchesini, L., Maximov, T. C., Maksyutov, S., and Schulze, E.-D.: An estimate of the terrestrial carbon budget of Russia using inventory-based, eddy covariance and inversion methods, *Biogeosciences*, 9, 5323–5340, <https://doi.org/10.5194/bg-9-5323-2012>, 2012.
- Eichler, A., Tinner, W., Brüttsch, S., Olivier, S., Papina, T., and Schwikowski, M.: An ice-core based history of Siberian forest fires since AD 1250, *Quaternary Sci. Rev.*, 30, 1027–1034, <https://doi.org/10.1016/j.quascirev.2011.02.007>, 2011.

- Fohlmeister, J., Arps, J., Spötl, C., Schröder-Ritzrau, A., Plessen, B., Günter, C., Frank, N., and Trüssel, M.: Carbon and oxygen isotope fractionation in the water-calcite-aragonite system, *Geochim. Cosmochim. Ac.*, 235, 127–139, <https://doi.org/10.1016/j.gca.2018.05.022>, 2018.
- Fohlmeister, J., Voarintsoa, N. R. G., Lechleitner, F. A., Boyd, M., Brandstätter, S., Jacobson, M. J., and L. Oster, J.: Main controls on the stable carbon isotope composition of speleothems, *Geochim. Cosmochim. Ac.*, 279, 67–87, <https://doi.org/10.1016/j.gca.2020.03.042>, 2020.
- Forkel, M., Thonicke, K., Beer, C., Cramer, W., Bartalev, S., and Schmullius, C.: Extreme fire events are related to previous-year surface moisture conditions in permafrost-underlain larch forests of Siberia, *Environ. Res. Lett.*, 7, 044021, <https://doi.org/10.1088/1748-9326/7/4/044021>, 2012.
- Gao, C., Zhao, F., Shi, C., Liu, K., Wu, X., Wu, G., Liang, Y., and Shu, L.: Previous Atlantic Multidecadal Oscillation (AMO) modulates the lightning-ignited fire regime in the boreal forest of Northeast China, *Environ. Res. Lett.*, 16, 024054, <https://doi.org/10.1088/1748-9326/abde09>, 2021.
- García-Lázaro, J. R., Moreno-Ruiz, J. A., Riaño, D., and Arbelo, M.: Estimation of Burned Area in the Northeastern Siberian Boreal Forest from a Long-Term Data Record (LTDR) 1982–2015 Time Series, *Remote Sens.-Basel*, 10, 940, <https://doi.org/10.3390/rs10060940>, 2018.
- Glückler, R., Herzschuh, U., Kruse, S., Andreev, A., Vyse, S. A., Winkler, B., Biskaborn, B. K., Pestryakova, L., and Dietze, E.: Wildfire history of the boreal forest of south-western Yakutia (Siberia) over the last two millennia documented by a lake-sediment charcoal record, *Biogeosciences*, 18, 4185–4209, <https://doi.org/10.5194/bg-18-4185-2021>, 2021.
- Glückler, R., Geng, R., Grimm, L., Baisheva, I., Herzschuh, U., Stoof-Leichsenring, K. R., Kruse, S., Andreev, A., Pestryakova, L., and Dietze, E.: Holocene wildfire and vegetation dynamics in Central Yakutia, Siberia, reconstructed from lake-sediment proxies, *Frontiers in Ecology and Evolution*, 10, 962906, <https://doi.org/10.3389/fevo.2022.962906>, 2022.
- Golubtsov, V. A., Cherkashina, A. A., Vanteeva, Yu. V., Voropay, N. N., and Turchinskaya, S. M.: Variations in the stable carbon isotopic composition of soil organic matter in mountain depressions of the Cis-Baikal region, *Contemp. Probl. Ecol.*, 16, 776–789, <https://doi.org/10.1134/S1995425523060094>, 2023.
- Granina, N. I., Martynova, N. A., and Kiseleva, N. D.: Spatio-temporal heterogeneity of soil cover in Baikal area and its impact on the development of agriculture in the region, *IOP C. Ser. Earth Env.*, 368, 012017, <https://doi.org/10.1088/1755-1315/368/1/012017>, 2019.
- Granoszewski, W., Demske, D., Nita, M., Heumann, G., and Andreev, A. A.: Vegetation and climate variability during the Last Interglacial evidenced in the pollen record from Lake Baikal, *Global Planet. Change*, 46, 187–198, <https://doi.org/10.1016/j.gloplacha.2004.09.017>, 2005.
- Hantemirov, R. M., Corona, C., Guillet, S., Shiyatov, S. G., Stoffel, M., Osborn, T. J., Melvin, T. M., Gorlanova, L. A., Kukarskih, V. V., Surkov, A. Y., von Arx, G., and Fonti, P.: Current Siberian heating is unprecedented during the past seven millennia, *Nat. Commun.*, 13, 4968, <https://doi.org/10.1038/s41467-022-32629-x>, 2022.
- Hedges, J. I. and Mann, D. C.: The characterization of plant tissues by their lignin oxidation products, *Geochim. Cosmochim. Ac.*, 43, 1803–1807, [https://doi.org/10.1016/0016-7037\(79\)90028-0](https://doi.org/10.1016/0016-7037(79)90028-0), 1979.
- Heidke, I., Scholz, D., and Hoffmann, T.: Quantification of lignin oxidation products as vegetation biomarkers in speleothems and cave drip water, *Biogeosciences*, 15, 5831–5845, <https://doi.org/10.5194/bg-15-5831-2018>, 2018.
- Hessilt, T. D., Abatzoglou, J. T., Chen, Y., Randerson, J. T., Scholten, R. C., van der Werf, G., and Veraverbeke, S.: Future increases in lightning ignition efficiency and wildfire occurrence expected from drier fuels in boreal forest ecosystems of western North America, *Environ. Res. Lett.*, 17, 054008, <https://doi.org/10.1088/1748-9326/ac6311>, 2022.
- Homann, J., Oster, J. L., de Wet, C. B., Breitenbach, S. F. M., and Hoffmann, T.: Linked fire activity and climate whiplash in California during the early Holocene, *Nat. Commun.*, 13, 7175, <https://doi.org/10.1038/s41467-022-34950-x>, 2022.
- Homann, J., Karbach, N., Carolin, S. A., James, D. H., Hodell, D., Breitenbach, S. F. M., Kwiecien, O., Brenner, M., Peraza Lope, C., and Hoffmann, T.: Past fire dynamics inferred from polycyclic aromatic hydrocarbons and monosaccharide anhydrides in a stalagmite from the archaeological site of Mayapan, Mexico, *Biogeosciences*, 20, 3249–3260, <https://doi.org/10.5194/bg-20-3249-2023>, 2023.
- Jex, C. N., Pate, G. H., Blyth, A. J., Spencer, R. G. M., Hernes, P. J., Khan, S. J., and Baker, A.: Lignin biogeochemistry: from modern processes to Quaternary archives, *Quaternary Sci. Rev.*, 87, 46–59, <https://doi.org/10.1016/j.quascirev.2013.12.028>, 2014.
- Kamp, U., Walther, M., and Dashtseren, A.: Mongolia's cryosphere, *Geomorphology*, 410, 108202, <https://doi.org/10.1016/j.geomorph.2022.108202>, 2022.
- Kharuk, V. I., Ponomarev, E. I., Ivanova, G. A., Dvinskaya, M. L., Coogan, S. C. P., and Flannigan, M. D.: Wildfires in the Siberian taiga, *Ambio*, 50, 1953–1974, <https://doi.org/10.1007/s13280-020-01490-x>, 2021.
- Kharuk, V. I., Shvetsov, E. G., Buryak, L. V., Golyukov, A. S., Dvinskaya, M. L., and Petrov, I. A.: Wildfires in the Larch Range within Permafrost, Siberia, *Fire*, 6, 301, <https://doi.org/10.3390/fire6080301>, 2023.
- Kılıç, G. M., Kashuba, N., Koptekin, D., Bergfeldt, N., Dönertaş, H. M., Rodríguez-Varela, R., Shergin, D., Ivanov, G., Kichigin, D., Pestereva, K., Volkov, D., Mandryka, P., Kharinskii, A., Tishkin, A., Ineshin, E., Kovychev, E., Stepanov, A., Dalén, L., Günther, T., Kirdök, E., Jakobsson, M., Somel, M., Krzewińska, M., Storå, J., and Götherström, A.: Human population dynamics and *Yersinia pestis* in ancient northeast Asia, *Science Advances*, 7, eabc4587, <https://doi.org/10.1126/sciadv.abc4587>, 2021.
- Klein Tank, A. M. G., Wijngaard, J. B., Können, G. P., Böhm, R., Demarée, G., Gocheva, A., Mileta, M., Pashiardis, S., Hejkrlik, L., Kern-Hansen, C., Heino, R., Bessemoulin, P., Müller-Westermeier, G., Tzanakou, M., Szalai, S., Pálsdóttir, T., Fitzgerald, D., Rubin, S., Capaldo, M., Maugeri, M., Leitass, A., Bukantis, A., Aberfeld, R., van Engelen, A. F. V., Forland, E., Mielus, M., Coelho, F., Mares, C., Razuvaev, V., Nieplova, E., Cegnar, T., Antonio López, J., Dahlström, B., Moberg, A., Kirchhofer, W., Ceylan, A., Pachaliuk, O., Alexander, L. V., and Petrovic, P.: Daily dataset of 20th-century surface air temperature and precip-

- itation series for the European Climate Assessment, *Int. J. Climatol.*, 22, 1441–1453, <https://doi.org/10.1002/joc.773>, 2002.
- Kobe, F., Bezrukova, E. V., Leipe, C., Shchetnikov, A. A., Goslar, T., Wagner, M., Kostrova, S. S., and Tarasov, P. E.: Holocene vegetation and climate history in Baikal Siberia reconstructed from pollen records and its implications for archaeology, *Archaeological Research in Asia*, 23, 100209, <https://doi.org/10.1016/j.ara.2020.100209>, 2020.
- Kobe, F., Hoelzmann, P., Gliwa, J., Olschewski, P., Peskov, S. A., Shchetnikov, A. A., Danukalova, G. A., Osipova, E. M., Goslar, T., Leipe, C., Wagner, M., Bezrukova, E. V., and Tarasov, P. E.: Lateglacial–Holocene environments and human occupation in the Upper Lena region of Eastern Siberia derived from sedimentary and zooarchaeological data from Lake Ochaul, *Quatern. Int.*, 623, 139–158, <https://doi.org/10.1016/j.quaint.2021.09.019>, 2022.
- Kostrova, S. S., Meyer, H., Fernandoy, F., Werner, M., and Tarasov, P. E.: Moisture origin and stable isotope characteristics of precipitation in southeast Siberia, *Hydrol. Process.*, 34, 51–67, <https://doi.org/10.1002/hyp.13571>, 2020.
- Kozlova, A. A., Belozertseva, I. A., Lopatina, D. N., Guzeeva, V. S., Kusraev, K. D., Kucherenko, I. M., and Korshunova, S. A.: Patterns of development and distribution of soil cover in Southern Predbaikalia, *IOP C. Ser. Earth Env.*, 629, 012012, <https://doi.org/10.1088/1755-1315/629/1/012012>, 2021.
- Laaha, G., Gauster, T., Tallaksen, L. M., Vidal, J.-P., Stahl, K., Prudhomme, C., Heudorfer, B., Vlnas, R., Ionita, M., Van Lanen, H. A. J., Adler, M.-J., Caillouet, L., Delus, C., Fendekova, M., Gailliez, S., Hannaford, J., Kingston, D., Van Loon, A. F., Mediero, L., Osuch, M., Romanowicz, R., Sauquet, E., Stagge, J. H., and Wong, W. K.: The European 2015 drought from a hydrological perspective, *Hydrol. Earth Syst. Sci.*, 21, 3001–3024, <https://doi.org/10.5194/hess-21-3001-2017>, 2017.
- Laskar, J., Robutel, P., Joutel, F., Gastineau, M., Correia, A. C. M., and Levrard, B.: A long-term numerical solution for the insolation quantities of the Earth, *Astron. Astrophys.*, 428, 261–285, <https://doi.org/10.1051/0004-6361:20041335>, 2004.
- Lechleitner, F. A., Mason, A. J., Breitenbach, S. F. M., Vaks, A., Haghypour, N., and Henderson, G. M.: Permafrost-related hiatuses in stalagmites: Evaluating the potential for reconstruction of carbon cycle dynamics, *Quat. Geochronol.*, 56, 101037, <https://doi.org/10.1016/j.quageo.2019.101037>, 2020.
- Lugina, K., Groisman, P., Vinnikov, K., Koknaeva, V., and Speranskaya, N.: Monthly Surface Air Temperature Time Series Area-Averaged Over the 30-Degree Latitudinal Belts of the Globe, <https://doi.org/10.3334/CDIAC/CLI.003>, 2006.
- Marlon, J. R.: What the past can say about the present and future of fire, *Quaternary Res.*, 96, 66–87, <https://doi.org/10.1017/qua.2020.48>, 2020.
- Masyagina, O. V. and Menyailo, O. V.: The impact of permafrost on carbon dioxide and methane fluxes in Siberia: A meta-analysis, *Environ. Res.*, 182, 109096, <https://doi.org/10.1016/j.envres.2019.109096>, 2020.
- Mensah, R. A., Jiang, L., Renner, J. S., and Xu, Q.: Characterisation of the fire behaviour of wood: From pyrolysis to fire retardant mechanisms, *J. Therm. Anal. Calorim.*, 148, 1407–1422, <https://doi.org/10.1007/s10973-022-11442-0>, 2023.
- Obu, J., Westermann, S., Bartsch, A., Berdnikov, N., Christiansen, H. H., Dashtseren, A., Delaloye, R., Elberling, B., Etzelmüller, B., Kholodov, A., Khomutov, A., Kääb, A., Leibman, M. O., Lewkowicz, A. G., Panda, S. K., Romanovsky, V., Way, R. G., Westergaard-Nielsen, A., Wu, T., Yamkhin, J., and Zou, D.: Northern Hemisphere permafrost map based on TTOP modelling for 2000–2016 at 1 km² scale, *Earth-Sci. Rev.*, 193, 299–316, <https://doi.org/10.1016/j.earscirev.2019.04.023>, 2019.
- Peel, M. C., Finlayson, B. L., and McMahon, T. A.: Updated world map of the Köppen-Geiger climate classification, *Hydrol. Earth Syst. Sci.*, 11, 1633–1644, <https://doi.org/10.5194/hess-11-1633-2007>, 2007.
- Ponomarev, E., I., Kharuk, V. I., and Ranson, K. J.: Wild-fires Dynamics in Siberian Larch Forests, *Forests*, 7, 125, <https://doi.org/10.3390/f7060125>, 2016.
- Schuur, E. A. G., Abbott, B. W., Commane, R., Ernakovich, J., Euskirchen, E., Hugelius, G., Grosse, G., Jones, M., Koven, C., Leshyk, V., Lawrence, D., Lorant, M. M., Mauritz, M., Olefeldt, D., Natali, S., Rodenhizer, H., Salmon, V., Schädel, C., Strauss, J., Treat, C., and Turetsky, M.: Permafrost and climate change: carbon cycle feedbacks from the warming Arctic, *Annu. Rev. Env. Resour.*, 47, 343–371, <https://doi.org/10.1146/annurev-environ-012220-011847>, 2022.
- Segato, D., Villoslada Hidalgo, M. D. C., Edwards, R., Barbaro, E., Vallelonga, P., Kjær, H. A., Simonsen, M., Vinther, B., Maffezzoli, N., Zangrando, R., Turetta, C., Battistel, D., Vésteinson, O., Barbante, C., and Spolaor, A.: Five thousand years of fire history in the high North Atlantic region: natural variability and ancient human forcing, *Clim. Past*, 17, 1533–1545, <https://doi.org/10.5194/cp-17-1533-2021>, 2021.
- Senande-Rivera, M., Insua-Costa, D., and Miguez-Macho, G.: Spatial and temporal expansion of global wildland fire activity in response to climate change, *Nat. Commun.*, 13, 1208, <https://doi.org/10.1038/s41467-022-28835-2>, 2022.
- Shichi, K., Takahara, H., Krivonogov, S. K., Bezrukova, E. V., Kashiwaya, K., Takehara, A., and Nakamura, T.: Late Pleistocene and Holocene vegetation and climate records from Lake Kotokel, central Baikal region, *Quatern. Int.*, 205, 98–110, <https://doi.org/10.1016/j.quaint.2009.02.005>, 2009.
- Shichi, K., Goebel, T., Izuho, M., and Kashiwaya, K.: Climate amelioration, abrupt vegetation recovery, and the dispersal of *Homo sapiens* in Baikal Siberia, *Science Advances*, 9, eadi0189, <https://doi.org/10.1126/sciadv.adi0189>, 2023.
- Shvetsov, E. G., Kukavskaya, E. A., Buryak, L. V., and Barrett, K.: Assessment of post-fire vegetation recovery in Southern Siberia using remote sensing observations, *Environ. Res. Lett.*, 14, 055001, <https://doi.org/10.1088/1748-9326/ab083d>, 2019.
- Simoneit, B. R. T., Schauer, J. J., Nolte, C. G., Oros, D. R., Elias, V. O., Fraser, M. P., Rogge, W. F., and Cass, G. R.: Levoglucosan, a tracer for cellulose in biomass burning and atmospheric particles, *Atmos. Environ.*, 33, 173–182, [https://doi.org/10.1016/S1352-2310\(98\)00145-9](https://doi.org/10.1016/S1352-2310(98)00145-9), 1999.
- Smith, A. C., Wynn, P. M., Barker, P. A., Leng, M. J., Noble, S. R., and Tych, W.: North Atlantic forcing of moisture delivery to Europe throughout the Holocene, *Sci. Rep.-UK*, 6, 24745, <https://doi.org/10.1038/srep24745>, 2016.
- Spötl, C.: A simple method of soil gas stable carbon isotope analysis, *Rapid Commun. Mass Sp.*, 18, 1239–1242, <https://doi.org/10.1002/rcm.1468>, 2004.
- Steffen, W., Rockström, J., Richardson, K., Lenton, T. M., Folke, C., Liverman, D., Summerhayes, C. P., Barnosky, A. D., Cornell,

- S. E., Crucifix, M., Donges, J. F., Fetzer, I., Lade, S. J., Scheffer, M., Winkelmann, R., and Schellnhuber, H. J.: Trajectories of the earth system in the Anthropocene, *P. Natl. Acad. Sci. USA*, 115, 8252–8259, <https://doi.org/10.1073/pnas.1810141115>, 2018.
- Sun, Q., Burrell, A., Barrett, K., Kukavskaya, E., Buryak, L., Kaduk, J., and Baxter, R.: Climate variability may delay post-fire recovery of boreal forest in southern Siberia, Russia, *Remote Sens.-Basel*, 13, 2247, <https://doi.org/10.3390/rs13122247>, 2021.
- Svendsen, J. I., Alexanderson, H., Astakhov, V. I., Demidov, I., Dowdeswell, J. A., Funder, S., Gataullin, V., Henriksen, M., Hjort, C., Houmark-Nielsen, M., Hubberten, H. W., Ingólfsson, Ó., Jakobsson, M., Kjær, K. H., Larsen, E., Lokrantz, H., Lunkka, J. P., Lyså, A., Mangerud, J., Matiouchkov, A., Murray, A., Möller, P., Niessen, F., Nikolskaya, O., Polyak, L., Saarnisto, M., Siegert, C., Siegert, M. J., Spielhagen, R. F., and Stein, R.: Late Quaternary ice sheet history of northern Eurasia, *Quaternary Sci. Rev.*, 23, 1229–1271, <https://doi.org/10.1016/j.quascirev.2003.12.008>, 2004.
- Swain, D. L.: A Shorter, Sharper Rainy Season Amplifies California Wildfire Risk, *Geophys. Res. Lett.*, 48, e2021GL092843, <https://doi.org/10.1029/2021GL092843>, 2021.
- Talucci, A. C., Loranty, M. M., and Alexander, H. D.: Siberian taiga and tundra fire regimes from 2001–2020, *Environ. Res. Lett.*, 17, 025001, <https://doi.org/10.1088/1748-9326/ac3f07>, 2022.
- Tarasov, P., Granoszewski, W., Bezrukova, E., Brewer, S., Nita, M., Abzaeva, A., and Oberhänsli, H.: Quantitative reconstruction of the last interglacial vegetation and climate based on the pollen record from Lake Baikal, Russia, *Clim. Dynam.*, 25, 625–637, <https://doi.org/10.1007/s00382-005-0045-0>, 2005.
- Tarasov, P., Bezrukova, E., Karabanov, E., Nakagawa, T., Wagner, M., Kulagina, N., Letunova, P., Abzaeva, A., Granoszewski, W., and Riedel, F.: Vegetation and climate dynamics during the Holocene and Eemian interglacials derived from Lake Baikal pollen records, *Palaeogeogr. Palaeoclimatol.*, 252, 440–457, <https://doi.org/10.1016/j.palaeo.2007.05.002>, 2007.
- Tarasov, P. E., Bezrukova, E. V., and Krivonogov, S. K.: Late Glacial and Holocene changes in vegetation cover and climate in southern Siberia derived from a 15 kyr long pollen record from Lake Kotokel, *Clim. Past*, 5, 285–295, <https://doi.org/10.5194/cp-5-285-2009>, 2009.
- Tchebakova, N. M., Parfenova, E., and Soja, A. J.: The effects of climate, permafrost and fire on vegetation change in Siberia in a changing climate, *Environ. Res. Lett.*, 4, 045013, <https://doi.org/10.1088/1748-9326/4/4/045013>, 2009.
- Tepley, A. J., Thomann, E., Veblen, T. T., Perry, G. L. W., Holz, A., Paritsis, J., Kitzberger, T., and Anderson-Teixeira, K. J.: Influences of fire–vegetation feedbacks and post-fire recovery rates on forest landscape vulnerability to altered fire regimes, *J. Ecol.*, 106, 1925–1940, <https://doi.org/10.1111/1365-2745.12950>, 2018.
- Tolstoy, P.: The Archaeology of the Lena Basin and Its New World Relationships, Part II, *Am. Antiquity*, 24, 63–81, <https://doi.org/10.2307/276742>, 1958.
- Tomshin, O. and Solovyev, V.: Spatio-temporal patterns of wildfires in Siberia during 2001–2020, *Geocarto Int.*, 37, 7339–7357, <https://doi.org/10.1080/10106049.2021.1973581>, 2022.
- Turney, C. S. M. and Jones, R. T.: Does the Agulhas Current amplify global temperatures during super-interglacials?, *J. Quaternary Sci.*, 25, 839–843, <https://doi.org/10.1002/jqs.1423>, 2010.
- Vaks, A., Gutareva, O. S., Breitenbach, S. F. M., Avirmed, E., Mason, A. J., Thomas, A. L., Osinzev, A. V., Kononov, A. M., and Henderson, G. M.: Speleothems reveal 500 000 year history of Siberian permafrost, *Science*, 340, 183–186, <https://doi.org/10.1126/science.1228729>, 2013.
- Vaks, A., Mason, A. J., Breitenbach, S. F. M., Kononov, A. M., Osinzev, A. V., Rosenshaft, M., Borshevsky, A., Gutareva, O. S., and Henderson, G. M.: Palaeoclimate evidence of vulnerable permafrost during times of low sea ice, *Nature*, 577, 221–225, <https://doi.org/10.1038/s41586-019-1880-1>, 2020.
- Walker, X. J., Baltzer, J. L., Cumming, S. G., Day, N. J., Ebert, C., Goetz, S., Johnstone, J. F., Potter, S., Rogers, B. M., Schuur, E. A. G., Turetsky, M. R., and Mack, M. C.: Increasing wildfires threaten historic carbon sink of boreal forest soils, *Nature*, 572, 520–523, <https://doi.org/10.1038/s41586-019-1474-y>, 2019.
- Weber, A. W., White, D., Bazaliiskii, V. I., Goriunova, O. I., Savel'ev, N. A., and Katzenberg, M. A.: Hunter–gatherer foraging ranges, migrations, and travel in the middle Holocene Baikal region of Siberia: Insights from carbon and nitrogen stable isotope signatures, *J. Anthropol. Archaeol.*, 30, 523–548, <https://doi.org/10.1016/j.jaa.2011.06.006>, 2011.
- Westerling, A. L., Hidalgo, H. G., Cayan, D. R., and Swetnam, T. W.: Warming and earlier spring increase western U. S. forest wildfire activity, *Science*, 313, 940–943, <https://doi.org/10.1126/science.1128834>, 2006.
- White, D., Preece, R. C., Shchetnikov, A. A., Parfitt, S. A., and Dlussky, K. G.: A Holocene molluscan succession from floodplain sediments of the upper Lena River (Lake Baikal region), Siberia, *Quaternary Sci. Rev.*, 27, 962–987, <https://doi.org/10.1016/j.quascirev.2008.01.010>, 2008.
- Zennaro, P., Kehrwald, N., McConnell, J. R., Schüpbach, S., Maselli, O. J., Marlon, J., Vallelonga, P., Leuenberger, D., Zangrando, R., Spolaor, A., Borrotti, M., Barbaro, E., Gambaro, A., and Barbante, C.: Fire in ice: two millennia of boreal forest fire history from the Greenland NEEM ice core, *Clim. Past*, 10, 1905–1924, <https://doi.org/10.5194/cp-10-1905-2014>, 2014.
- Zhang, P., Jeong, J.-H., Yoon, J.-H., Kim, H., Wang, S.-Y. S., Linderholm, H. W., Fang, K., Wu, X., and Chen, D.: Abrupt shift to hotter and drier climate over inner East Asia beyond the tipping point, *Science*, 370, 1095–1099, <https://doi.org/10.1126/science.abb3368>, 2020.